

# Improvement of Fracture Toughness Lanthanum Zirconate

LI J Y<sup>1,2</sup>, DAI H<sup>1,2</sup>, LI Q<sup>1,2</sup>, ZHONG X H<sup>1,2</sup>, CAO X Q<sup>1\*</sup>

(1 Key Lab of Rare Earth Chemistry and Physics, Changchun Institute of Applied Chemistry, Chinese Academy of Sciences, Changchun 130022, China; 2 Graduate School of the Chinese Academy of Sciences, Beijing 100049, China)

**Abstract:**  $\text{La}_2\text{Zr}_2\text{O}_7$  (LZ) is a promising thermal barrier coating material for the high temperature applications. The fracture toughness and microhardness of nanocrystalline LZ (n-LZ), microcrystalline LZ (m-LZ) and LZ-5mol% 8YSZ (LZ-5-8YSZ) composite (8YSZ for zirconia stabilized by 8 mol% yttria) were studied. The n-LZ had a thermal expansion coefficient of  $(9.6 \pm 0.4) \times 10^{-6} \text{ K}^{-1}$  (200~1000°C) and fracture toughness of  $(1.98 \pm 0.07) \text{ MPa} \cdot \text{m}^{1/2}$  which are obviously higher than those of the m-LZ ( $(9.1 \pm 0.4) \times 10^{-6} \text{ K}^{-1}$  and  $(1.40 \pm 0.23) \text{ MPa} \cdot \text{m}^{1/2}$ , respectively), indicating that nanofication was an efficient way to increase the toughness and thermal expansion coefficient of LZ. The composite LZ-5-8YSZ had a higher fracture toughness ( $(1.88 \pm 0.30) \text{ MPa} \cdot \text{m}^{1/2}$ ) than LZ, which was close to that of 8YSZ densified by superhigh pressure (SHP).

**Key words:** ceramics; nanostructure; fracture toughness; thermal expansion

**CLC number:** TB331 **Document code:** A **Article ID:** 1001-4381(2006)05-0051-06

Thermal barrier coatings (TBCs) have found an increasing number of applications in protecting high-temperature metallic components, for example, TBCs are deposited on transition pieces, combustion lines, first-stage blades and vanes, and other hot-path components of gas turbines either to increase the inlet temperature with a consequent improvement of the efficiency or to reduce the requirements for a cooling system<sup>[1]</sup>. There are several ceramics that have been evaluated as TBC materials<sup>[2]</sup>. Lanthanum zirconate was recently proposed as a promising TBC material<sup>[2-8]</sup>. The properties of high melting point, phase stability up to its melting point, low thermal conductivity, low sintering ability and oxygen non-transparent are the major reasons that it is believed to have potential as TBC material for high temperature applications. However, its practical applications are limited by two problems, *i. e.*, the relatively low thermal expansion coefficient and low fracture toughness. The substitution of  $\text{ZrO}_2$  by  $\text{CeO}_2$  can largely improve the thermal expansion coefficient and the thermal cycling life of the coating is also largely im-

proved<sup>[9]</sup>.

Two methods are used to toughen LZ. The first one relies on the small particle size. It is generally known that nanocrystalline materials, which are structurally characterized by ultrafine grains and a large volume fraction of interfaces, have drawn increasing attention in recent years<sup>[10-14]</sup>. Due to the high density of interfaces and nano-size effect, nanocrystalline materials exhibit apparently different (usually enhanced) physical, chemical, and mechanical properties from those of either the conventional polycrystalline or the amorphous state. The nanocrystalline  $\text{TiO}_2$  shows the plastic deformation by indenting at ambient temperature. Chen and co-workers reported that the plasma-sprayed nanostructural zirconia coating has a higher thermal expansion coefficient than the traditional zirconia coating<sup>[11]</sup>. K. Lu and M. L. Sui reported that the linear thermal expansion coefficient increases markedly with a reduction of the average grain size in the nanocrystalline Ni-P alloys<sup>[12]</sup>. The second one is based on a phase change from the tetragonal  $\text{ZrO}_2$  to the monoclinic

**Foundation items:** supported by the NSFG-20471058 and “CAS-Bairen”.

\* **E-mail:** xcao@ciac.jl.cn.

$\text{ZrO}_2$ <sup>[15-18]</sup>. There are three types of phase for  $\text{ZrO}_2$ , *i. e.*, monoclinic (m), tetragonal (t) and cubic (c). The m-phase is the stable phase at room temperature. If the t-phase can be introduced as inclusions of small size, it can be retained to room temperature. It can then transform under stress associated with the growth of cracks to the m-phase. As a consequence of the volume dilatation during the t-phase to transformation ( $\Delta V = 4.7\%$  in the absence of constraints<sup>[16]</sup>), this phase transformation can arrest the crack growth and thus strengthen the material.<sup>[17,18]</sup> Although there is currently no exact correlation between microstructure, zone size and R-curve behavior, it has long been recognized that the selected heat treatments can be used to influence the transformation tendency of the t-phase precipitates and hence the transformation toughening of the material.

## 1 Experimental

### 1.1 Sample Preparation

The nano-powder of LZ was prepared using a modified sol-gel method<sup>[19]</sup>. Small pieces of round-shape samples with a diameter of 11 mm were obtained by pressing LZ nano-powder under a pressure of 0.3 GPa at room temperature. Such small pieces were further densified by SHP under a pressure of 4.5 GPa at 1000 °C for 10 min ( $6 \times 800$  Ton 6-axial presser, the prospect machine factory of Hebei Zhang Jia Kou). Such a high pressure for a short period would not bring to the grain growth of the nano-materials. The sample densified by SHP normally has a density above 95% of the theoretical value but the grain size is not obviously changed.

The preparation of 8YSZ nano-powder was the same as LZ. 5mol% 8YSZ powder was added into the LZ powder followed by grinding in an agate mortar for 20 min. LZ, 8YSZ and the mixture of LZ and 8YSZ powders were densified by SHP at 1450 °C for 10 min respectively.

### 1.2 Microstructure Analysis and Mechanical Property

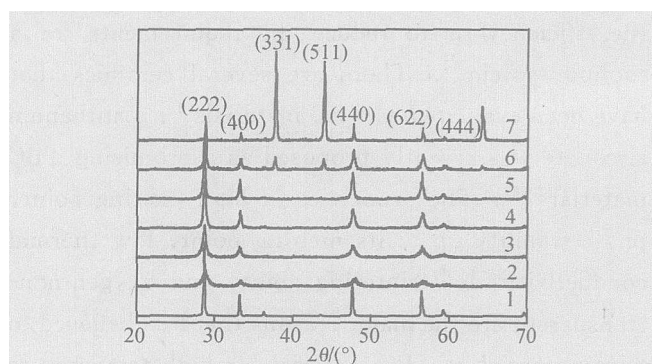
X-ray diffraction (XRD) patterns were collected on a Rigaku D/MaX-IIIB diffractometer with  $\text{Cu-K}\alpha$  radiation (0.15406 nm). The morphology of the LZ

nanopowder and the microstructure of the densified samples were analyzed by the scanning electron microscope (SEM, XL 30 ESEM FEG, Micro FEI Philips). A small bar with a dimension of  $2\text{mm} \times 1\text{mm} \times 4\text{mm}$  was used for the measurement of thermal expansion coefficient (TEC, Netzsch DIL-402C). Before the indentation test, the surfaces of the densified samples were polished with diamond suspensions (Metadi Diamond 15  $\mu\text{m}$  to 1  $\mu\text{m}$ , Buehler) by a low-speed automatic polisher (Minimet 1000, Buehler). The fracture toughness and Vicker's hardness were measured by a microindenter (Tukon 2100) with a load of 19.6N or 49.0N for 10s.

## 2 Results and Discussion

### 2.1 n-LZ

The XRD patterns of LZ powder after calcination at various temperatures are shown in Fig. 1. All the calcined powders and the sample densified by SHP show weak and broad peaks, indicating that the samples still keep the fine size below 1000 °C. The powders calcined at 800 °C for 24 h and 1000 °C for 12h have mean grain sizes of 13 nm and 34 nm respectively as calculated with the Scherrer's equation based on their XRD patterns<sup>[19]</sup>.



1-synthesized by the conventional solid state reaction at 1400 °C for 12h, n-LZ obtained by Sol-Gel method after calcination at various temperatures or densification by SHP; 2-800 °C, 24h; 3-900 °C, 24h; 4-1000 °C, 6h; 5-1000 °C, 12h; 6-densified by SHP; 7-densified by SHP and then heated from 35 °C to 1400 °C

Fig. 1 The XRD patterns of LZ powders

It is reported in ref. [20] that the binary oxides of rare earths with zirconia have two types of structures, *i. e.*, pyrochlore ( $\text{La}_2\text{O}_3$ ,  $\text{Pr}_6\text{O}_7 \sim \text{Gd}_2\text{O}_3$ ) and

fluorite ( $\text{Y}_2\text{O}_3$ ,  $\text{Th}_2\text{O}_3 \sim \text{Lu}_2\text{O}_3$ ). The fully-crystallized LZ has a pyrochlore structure which is very similar to that of the fluorite structure and the two weak peaks of  $2\theta$  between  $35^\circ$  (peak [331]) and  $45^\circ$  (Peak [511]) are the indication of pyrochlore structure<sup>[4,9]</sup>. Patterns 2 and 3 in Fig. 1 do not have these two peaks, and only above  $1000^\circ\text{C}$  as shown in Patterns 4  $\sim$  6 appear these two peaks, implying that LZ has two polymorphs with a phase-transition temperature of about  $1000^\circ\text{C}$  and the pyrochlore structure is more stable than the fluorite structure for LZ. By solid-state reaction, in other words, the reaction of the micro-sized  $\text{La}_2\text{O}_3$  with  $\text{ZrO}_2$ , the formation of LZ can only be finished above  $1400^\circ\text{C}$  and only the pyrochlore structure can be obtained. The densification by SHP at  $1000^\circ\text{C}$  for a short time also brings to the formation of pyrochlore as shown in pattern 5. On the other hand, it is interesting to find that after SHP especially after further annealing, peaks [331] and [511] are much stronger than those of the calcined samples, indicating that the crystal growth under SHP is oriented. As reported in ref. [4], during annealing or thermal cycling, the crystal growth in the as-prepared coating of LZ is also oriented and Peak [400] is the most favored.

The fracture surface of n-LZ densified by SHP is shown in Fig. 2. The grain size is about 20 nm which is consistent with the result obtained by XRD.

In Fig. 3 are shown the TECs of both n-LZ and m-LZ as a function of temperature for comparison. The averaged TEC of n-LZ between  $200^\circ\text{C}$  and  $1000^\circ\text{C}$  has an obviously higher value ( $(9.6 \pm 0.4) \times 10^{-6} \text{ K}^{-1}$ ) than the m-LZ ( $(9.1 \pm 0.4) \times 10^{-6} \text{ K}^{-1}$ ). The enhancement of TEC by nanofication has already been observed for the metallic materials such as Cu, Pd, Ni-P and so on<sup>[12, 21]</sup>. The enhanced TEC of nanocrystalline materials is usually attributed to the increased grain-boundary component in the nanostructures<sup>[21]</sup>. By describing the nanocrystalline material as a two-component system with a crystallite component and a grain boundary (or interface) one, the TEC can be estimated by appropriate scaling of the grain boundary contribution<sup>[12]</sup>. Nanocrystalline with ultrafine grain has a large volume fraction of interfaces. There is a difference between the TECs of

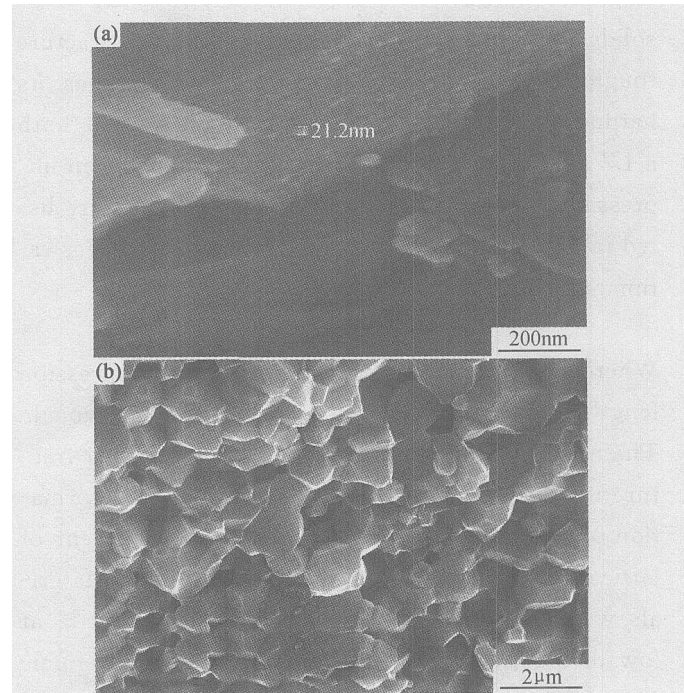


Fig. 2 SEM photographs of the fracture surface of n-LZ (a) and m-LZ (b)

the interface and crystalline, and the TECs of the interfaces are usually several times that for the crystalline state depending on the material and the grain size<sup>[12]</sup>, and the grain-size dependence of TEC usually obeys the  $D^{-1}$ -rule ( $D$  is the mean grain size). In the temperature range of  $100 \sim 500^\circ\text{C}$ , the averaged TECs of  $\alpha$ -alumina are  $5.93 \times 10^{-6}$ ,  $5.59 \times 10^{-6} \text{ K}^{-1}$  and  $9.88 \times 10^{-6} \text{ K}^{-1}$  for the grain sizes of  $5 \mu\text{m}$ ,  $105 \text{ nm}$  and  $80 \text{ nm}$ , respectively<sup>[22]</sup>, indicating that the grain-size effect on TEC becomes obvious only when the size is below  $100 \text{ nm}$  for this material.

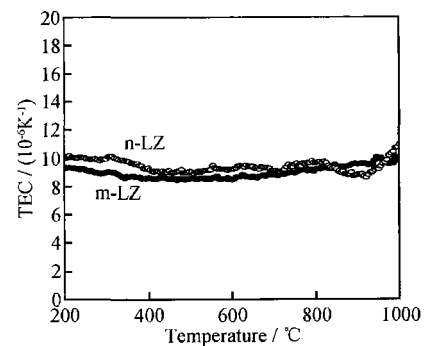


Fig. 3 Thermal expansion coefficients of n-LZ and m-LZ as a function of temperature

A small grain size is known to have a strong influence on the mechanical properties which may be superior to those of the conventional polycrystalline

solids, and it is also well known that the fracture toughness of a material generally decreases as its hardness increases<sup>[23]</sup>. Vicker's hardnesses of both  $\alpha$ -LZ and  $m$ -LZ are measured and the indentation impressions are shown in Fig. 4 and the results are listed in Table 1. The fracture toughness ( $K_{IC}$ ) was estimated from the crack length<sup>[24]</sup>:

$$K_{IC} = 0.16Ha^{1/2}(c/a)^{-2/3}$$

Where  $H$  is hardness,  $2c$  is the crack and impression length and  $2a$  is the length of the indent diagonal. The  $\alpha$ -LZ has a lower hardness and much higher fracture toughness than the  $m$ -LZ. The plastic deformation of crystalline solids occurs by the movement of lattice dislocations and/or diffusional creep. Materials with immobile lattice dislocations are brittle at low temperatures, and this applies to most ceramic materials. However, if the grain size of the ceramic material is reduced to the nano-size, even the brittle ceramic becomes ductile at a low temperature which is much lower than its melting point<sup>[10]</sup>, and the ductility seems to originate from the diffusional flow of atoms along the intercrystalline interfaces of the nanograins. The deformation rate  $\dot{\epsilon}$  of diffusional creep of a polycrystalline material has a relation of  $\dot{\epsilon} \sim D^{-3}$  ( $D$  is the grain size), and accordingly the reduction of grain size has a strong effect on the enhancement of the toughness.

**Table 1 Comparison of the mechanic properties of the  $\alpha$ -LZ,  $m$ -LZ, LZ-5-8YSZ and 8YSZ**

Material	HV/ GPa <sup>①</sup>	$K_{IC}$ / (MPa $\cdot$ m <sup>1/2</sup> ) <sup>②</sup>	TEC/ ( $\times 10^{-6}$ K <sup>-1</sup> , 200~1000℃) <sup>③</sup>
$\alpha$ -LZ	7.41 $\pm$ 0.19	1.98 $\pm$ 0.07	9.6 $\pm$ 0.4
$m$ -LZ	8.47 $\pm$ 1.18	1.40 $\pm$ 0.23	9.1 $\pm$ 0.4
LZ-5-8YSZ	6.07 $\pm$ 0.24	1.88 $\pm$ 0.30	9.1 $\pm$ 0.4
8YSZ	8.23 $\pm$ 0.64	1.80 $\pm$ 0.12	11.0 $\pm$ 0.4

① HV, Vicker's hardness; ②  $K_{IC}$ , fracture toughness; ③ TEC, thermal expansion coefficient

The crack propagation behavior around the Vicker's indentation for both  $\alpha$ -LZ and  $m$ -LZ are shown in Fig. 5. The crack path of  $\alpha$ -LZ is not straight and has a broadness of about 0.5~1  $\mu$ m (Fig. 5a, b). Due to the smaller size of the nanograin, it is difficult to determine whether the fracture is transgranular or intergranular as shown in Fig. 2.

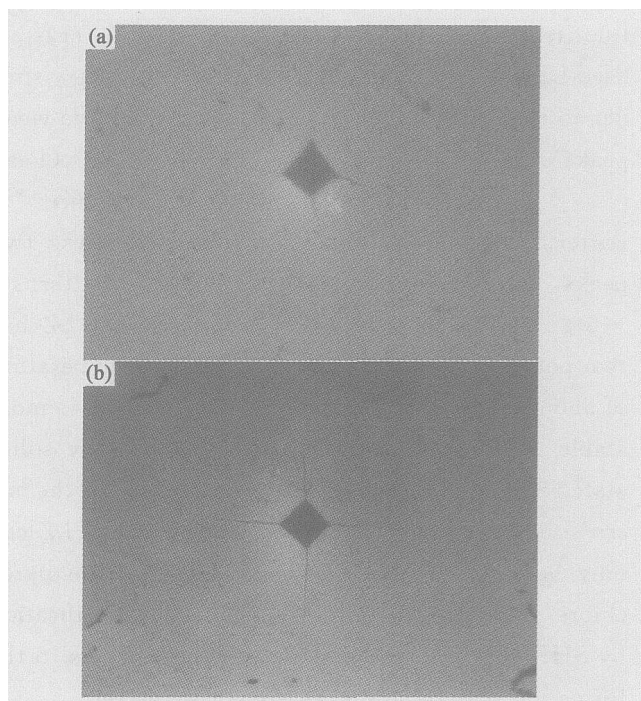


**Fig. 4 Hardness test impressions of  $\alpha$ -LZ (a) and  $m$ -LZ (b)**

However, for  $\alpha$ -LZ the crack propagates with microscopical deflection and bridging of the crack can be observed obviously. Crack deflection and crack bridging are two important toughening mechanisms for ceramic materials. Crack deflection is the defined microstructural elements which lead to an increase of fracture toughness at the crack tip; crack bridging is described as the process where microstructural elements connect both crack faces and transmit a closure force across the crack walls, which, by definition, occurs behind the crack tip and leads to a crack-length dependent fracture toughness ( $R$ -curve)<sup>[25]</sup>. Compared with the crack of  $\alpha$ -LZ, the crack deflection of  $m$ -LZ is not obvious (Fig. 5c). The crack deflection is therefore thought to be an important reason of toughness increment of  $\alpha$ -LZ. For the nanocrystalline FeMoSiB/Ni laminate composite, the toughness can be improved by the crack deflection<sup>[26]</sup>, and for the nanostructured WC-Co composites bridging is a more important toughening mechanism than the plastic deformation<sup>[23]</sup>. For the  $\alpha$ -LZ ceramic material, even though no further proof is available to determine which mechanism is dominant, however, bridging obviously makes contribution to the increase of toughness.

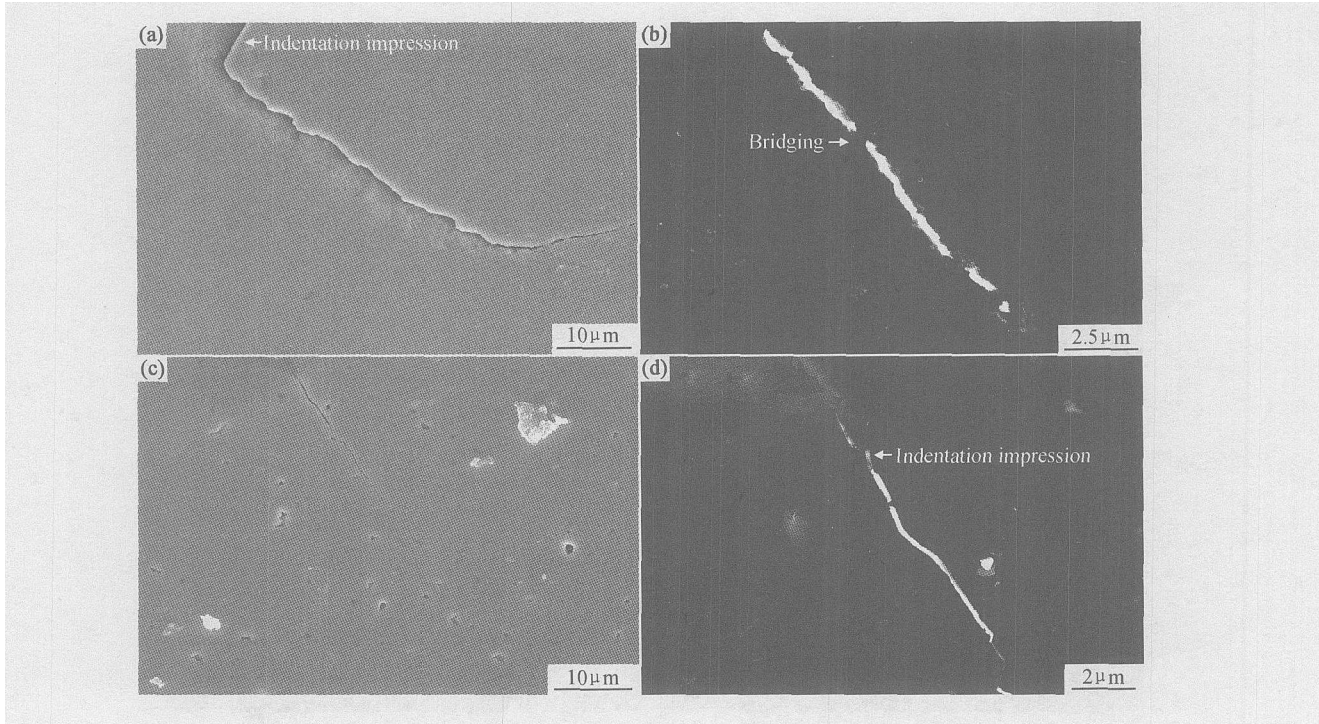
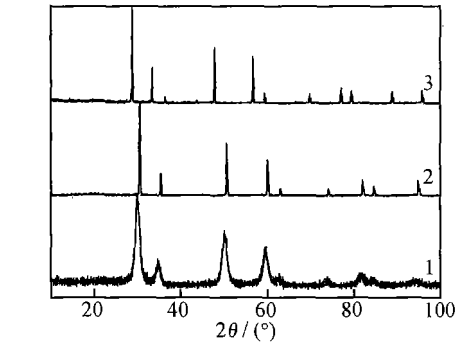


Fig. 5 The SEM photographs of the crack of  $m$ -LZ (a, b) and  $m$ -LZ (c, d) after indentation test

2.2 LZ+ 8YSZ

The XRD patterns of the 8YSZ and LZ powder which were densified by SHP under a pressure of 4.5 GPa at 1450 °C for 10 min and heated at 1450 °C for 1h are shown in Fig. 6. Only the  $t$ -phase was observed in the XRD pattern of the 8YSZ powder obtained by sol-gel method and calcined at 600 °C for 20h (Fig. 6. 1), which shows weak and broadened peaks and the powder still keeps the nano-size of about 10 nm. After being densified by SHP (Fig. 6. 2), 8YSZ still keeps the tetragonal structure, indicating that such a high pressure for a short period at 1450 °C would suppress the transformation of  $t$ -ZrO<sub>2</sub> to  $m$ -ZrO<sub>2</sub>. The SHP could be an effective method that keeps the  $t$ -phase for zirconia at room temperature. It is benefit to enhance the fracture toughness of ceramics by transformation toughening of ZrO<sub>2</sub>.

Vicker’s hardness and fracture toughness of LZ-5-8YSZ composite are shown in Table 1. The composite LZ-5-8YSZ has a fracture toughness of 1.88 MPa • m<sup>1/2</sup> which is obviously higher than that of LZ and close to that of 8YSZ. The sintered pellets are carefully polished and the SEM images of the sample surfaces are compared in Fig. 7a, b. The microstructure of composite LZ-5-8YSZ is quite different from



1- the 8YSZ nanopowder obtained by Sol-Gel method after calcination at 600 °C for 20 h; 2- the 8YSZ and 3-the LZ densified by SHP and then heated at 1450 °C for 1h

Fig. 6 The XRD patterns of LZ and 8YSZ powders

that of LZ. The rod-like particles are observable in LZ-5-8YSZ, which is consistent with the SEM observation of the fracture surface. The range of these rod-like particles is not regular and the dimensions of these rod-like particles are approximately 1000 nm long and 400 nm wide. The SEM pictures of the freshly cleaved surfaces of LZ and LZ-5-8YSZ are shown in Figures 7c, d. In Fig. 7c it is noted that the fracture of LZ is obviously intergranular, and the LZ-5-8YSZ is transgranular. This would be the reason of higher toughness for LZ-5-8YSZ<sup>[27]</sup>.

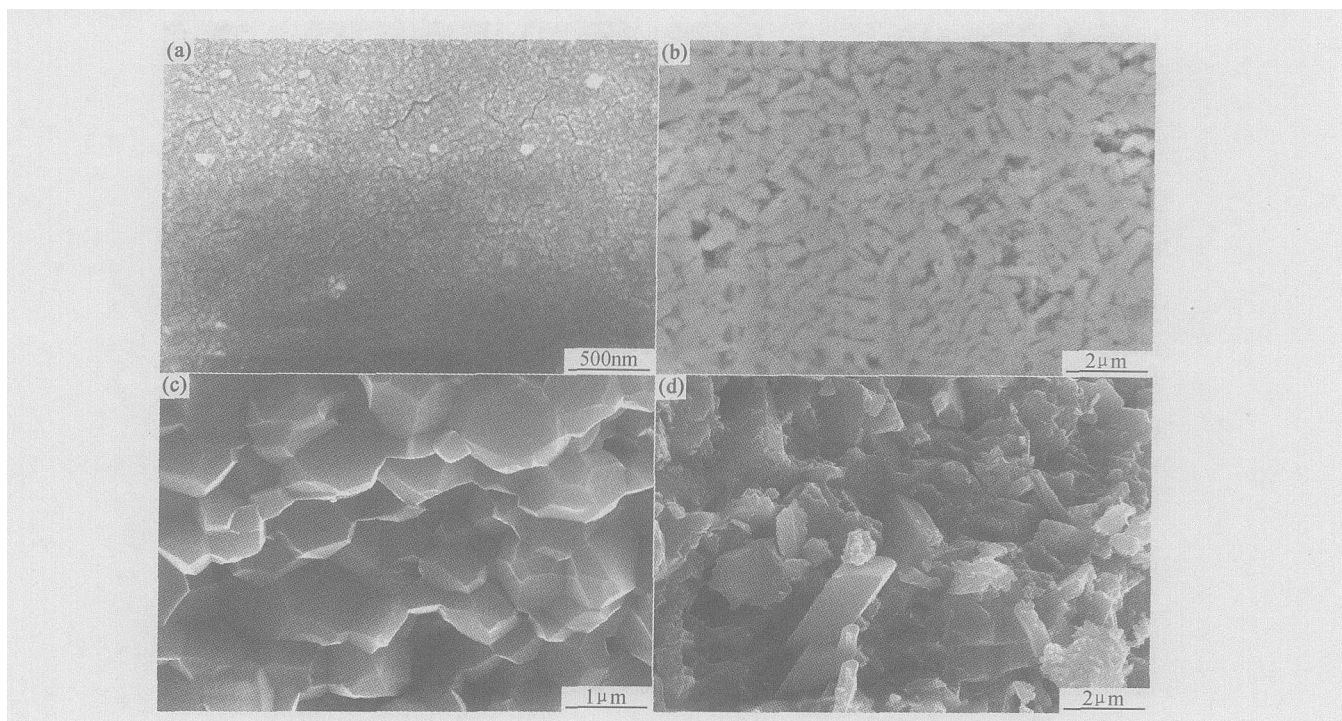


Fig. 7 The SEM images of LZ and LZ-5-8YSZ (a) the polished surface of LZ; (b) the polished surface of LZ-5-8YSZ; (c) and (d) are the fractured surfaces of (a) and (b), respectively

### 3 Conclusion

The study of this work indicates that, in order to keep the nano-grains, SHP is a good choice for the sintering of nano-materials, and nanofication is really an efficient way for the improvement of thermal expansion coefficient and fracture toughness which are two of the most important properties for the TBC materials. The LZ-5-8YSZ has a rod-shape structure and the fracture was transgranular, obviously improving the toughness of LZ.

#### References:

- [1] CERNUSCHI F, BIANCHI P, LEONI M, et al. Thermal diffusivity/microstructure relationship in Y-PSZ thermal barrier coating [J]. *J Therm Spray Technol*, 1999, 8 (1): 102–109.
- [2] CAO X Q, VASSEN R, STOEVEER D. Ceramic materials for thermal barrier coatings [J]. *J Europ Ceram Soc*, 2004, 24 (1): 1–10.
- [3] VASSEN R, CAO X Q, TIETZ F. In Proceedings of the United Thermal Spray Conference '99 [C]. Düsseldorf Germany: ASM International, Verlag fuer Schweißen und Verwandte Verfahren, Duesseldorf, 1999. 830–834.
- [4] VASSEN R, CAO X Q, TIETZ F, et al. Zirconates as new materials for thermal barrier coatings [J]. *J Am Ceram Soc*, 2000, 83 (8): 2023–2028.
- [5] CAO X Q, VASSEN R, JUNG W, et al. Thermal stability of lanthanum zirconate plasma-sprayed coating [J]. *J Am Ceram Soc*, 2001, 84 (9): 2086–2090.
- [6] VASSEN R, TIETZ F, KERKHOFF G, et al. In Proceedings of the 6th Liege Conference on Materials for Advanced Powder Engineering [C]. Universite de Liege, Belgium: Forschungszentrum Juelich GmbH, Deutschland, 1998. 1627–1635.
- [7] VASSEN R, CAO X Q, DIETRICH M, et al. In The 25th Annual International Conference on Advanced Ceramics and Composites: An Advanced Ceramics Odyssey [C]. Cocoa Beach of Florida: Am Ceram Soc, 2001. 435–443.
- [8] MICHAEL MALONEY J. Thermal barrier coating systems and materials [P]. Europ Patent: EP 0848077 A1, 1998.
- [9] CAO X Q, VASSEN R, FISCHER W, et al. Lanthanum-cerium oxide as a thermal barrier coating material for high-temperature applications [J]. *Adv Mater*, 2003, 15 (17): 1438–1441.
- [10] KARCH J, BIRRINGER R, GLEITER H. Ceramics ductile at low temperature [J]. *Nature*, 1987, 330 (6147): 556–558.
- [11] CHEN H, ZHOU X M, DING CH X. Investigation of the thermomechanical properties of a plasma-sprayed nanostructured zirconia coating [J]. *J Europ Ceram Soc*, 2003, 23: 1449–1455.
- [12] LU K, SUIM L. Thermal expansion behaviors in nanocrystalline materials with a wide grain size range [J]. *Acta Metall Mater*, 1995, 43 (9): 3325–3332.
- [13] EIDEN-ASSMANN S, MARET G. CeF<sub>3</sub> nanoparticles: synthesis and characterization [J]. *Mater Res Bull*, 2004, 39: 21–24.
- [14] MENZLER N H, LAVERGNAT D, TIETZ F, et al. Materials synthesis and characterization of 8YSZ nanomaterials for the fabrication of electrolyte membranes in solid oxide fuel cells [J]. *Ceram Intern*, 2003, 29: 619–628.

to the vitrification, where a transition to a glassy solid is made. The reaction is very slow thereafter. Between  $T_{g1}$  and  $T_{g\infty}$ , the solution ends the possibility of flow. Crosslinking continues at a good rate until vitrification.

### 3 Conclusions

The cure kinetics of a bicomponent high performance epoxy resin was studied by dynamic DSC analysis, and the parameters of the cure reaction were obtained to establish a phenomenological model. The relationship between glass transition temperature ( $T_g$ ) and cure degree ( $\alpha$ ) was analyzed with isothermal plus dynamic DSC method based on DiBenedetto equation, a mathematical description of  $T_g$  as a function of both time and temperature was suggested. Round disk compression mode DMA was employed to study the gelation at different temperatures, the relationship between gel time and temperature was obtained. The conversion at gelation was turned out to be  $\alpha = 0.4539$ , while the temperature at which vitrification line and gelation line transected was found to be  $T_{gd} = 70.18^\circ\text{C}$ . The Time-Temperature-Transition (TTT) diagram was plotted based on the works above, which served as a tool for process optimization in advanced composites manufacture.

### Acknowledgements

The work was supported by National Basic Research Program (the 973 program) under the grant No. of 2003CB615604, and the NNSF Key Basic Research Project under the grant No. of 10590356. Mrs. CHEN Tao and Mrs. CUI Yu are highly acknowledged for their support in the experiment.

### References:

- [1] RUDD C D, LONG A C, KENDALL K N, et al. Liquid molding technologies [M]. Woodhead Publishing Ltd, 1997. 84– 87.
- [2] GAO Jia-wu, SHEN Kui, GAO Zong-meng. The cure behavior of tetraglycidyl diaminodiphenyl methane with diaminodiphenyl sulfone [J]. *Thermochimica Acta*, 2000, 352– 353: 153– 158.
- [3] NÚÑEZ L, FRAGA F, CASTRO A, et al. TTT cure diagram for an epoxy system diglycidyl ether of bisphenol A/1,2 diamine cyclohexane/ calcium carbonate filler [J]. *Polymer*, 2001, 42: 3581– 3587.
- [4] ROSU D, MUSTATĂ F, CASCAVAL C N. Investigation of the

curing reactions of some multifunctional epoxy resins using differential scanning calorimetry [J]. *Thermochimica Acta*, 2001, 370, 105– 110.

- [5] H KUN HSEIH, CHEAN C S U, EAM O R M W O O. Cure kinetics and inter-domain etherification in an amine cured phenoxy/epoxy system [J]. *Polymer*, 1998, 39(11): 2175– 2183.
- [6] J LÓPEZ, I LÓPEZ BUENO, P NOGUEIRA, et al. Effect of poly(styrene-co-acrylonitrile) on the curing of an epoxy/amine resin [J]. *Polymer*, 2001, 42: 1669– 1677.
- [7] G VAN ASSCHE, A VAN HEMELRIJCK, H RAHIER, et al. Modulated temperature differential scanning calorimetry: cure, vitrification, and devitrification of thermosetting systems [J]. *Thermochimica Acta*, 1997, 304– 305: 317– 334.
- [8] G VAN ASSCHE, S SWIER, B VAN MELE. Modeling and experimental verification of the kinetics of reacting polymer systems [J]. *Thermochimica Acta*, 2002, 388: 327– 341.

(上接第 56 页)

- [15] GARIVER C, HANNINK R H, PASCOE R T. Ceramic steel [J]. *Nature*, 1975, 258: 703– 704.
- [16] RUHLE M, HEUER A H. In Science and Technology of Zirconia II, *Advances in Ceramics* [M]. Columbus: Am Ceram Soc, 1984.
- [17] HANNINK R H J, KELLY P M, MUDDLE B C. Transformation toughening in zirconia-containing ceramics [J]. *J Am Ceram Soc*, 2000, 83(3): 461– 487.
- [18] LANGE F F. Transformation toughening, part 2: contribution to fracture toughness [J]. *J Mat Sci*, 1982, 17: 235– 239.
- [19] RAO K K, BANU T, VITHAL M, et al. Preparation and characterization of bulk and nano particles of  $\text{La}_2\text{Zr}_2\text{O}_7$  and  $\text{Nd}_2\text{Zr}_2\text{O}_7$  by sol-gel method [J]. *Mater Lett*, 2002, 54: 205– 210.
- [20] SUBRAMANIAN M A, ARAVAMUDAN G, SUBBA RAO G V. Oxide pyrochlores—a review [J]. *Prog Solid State Chem*, 1983, 15: 55– 143.
- [21] ZHAO Y H, LU K. Grain size dependence of thermal properties of nanocrystalline elemental selenium studied by X-ray diffraction [J]. *Phy Rev B*, 1997, 56(14): 330.
- [22] CAO M S, JIANG C Y, TIAN Y J. Introduction to the Nanomaterials [M]. Harbin: The Publishing House of Harbin Engineering University, 2001. 89– 94.
- [23] JIA K, FISCHER T E, GALLOIS B. Microstructure, hardness and toughness of nanostructured and conventional WC-Co composites [J]. *Nanostruct Mater*, 1998, 10(5): 875– 891.
- [24] EVANS A G, CHARLES E A. Fracture toughness determination by indentation [J]. *J Am Ceram Soc*, 1976, 7– 8(59): 371– 372.
- [25] RODEL J. Interaction between crack deflection and crack bridging [J]. *J Europ Ceram Soc*, 1992, 10: 143– 150.
- [26] GAN Y, ZHOU B L. Nanocrystalline FeMnSiB/Ni laminate composite—preparation and mechanical properties [J]. *Mater Lett*, 2002, 55: 296– 299.
- [27] KWON N H, KIM G H, SONG H S, et al. Synthesis and properties of cubic zirconia-alumina composite by mechanical alloy [J]. *Mater Sci Eng A*, 2001, 299: 185– 194.